Helena Geirinhas RAMOS[1], Artur Lopes RIBEIRO[1], Michal KUBÍNYI[2]

Instituto de Telecomunicações, IST, Lisboa, Portugal (1), Czech Technical University in Prague, Faculty of Electrical Engineering, Prague, Czech Republic (2)

Measuring interface for an ECT System

Abstract. *This paper describes the measuring interface to be included in an automated microcomputer based Eddy Current Testing (ECT) system developed to characterize structural flaws inside electrically conducting nonmagnetic plates. The principle of operation is based on the measurement of the output voltages of two sensing coils. A description of the implemented prototype using two different types of probes including the digital signal processing used to overcome the signal degradation is presented. The application of a 2D Finite Element Method (FEM) allows to preview the range of the resulting output voltages in the detection coils and also the excitation current amplitude necessary to obtain a given signal to noise ratio. The experimental results obtained with the two probes are presented and one may conclude by inspection that the quality of the obtained data and the amount of information required for future structural defects characterization depend greatly on the probe geometry.*

Streszczenie. *W artykule opisano interfejs stosowany w mikrokomputerowym systemie pomiarowym wykorzystującym prądy wirowe. System służy do badania materiałów niemagnetycznych. Do pomiaru służą dwie cewki otaczające próbkę. Badania eksperymentalne potwierdziły że jakość badania struktury silnie zależy od geometrii próbki.* ***(Interfejs pomiarowy w systemie wykorzystującym prądy wirowe****)*

Keywords: Electromagnetic non-destructive testing, finite element method, eddy currents, inductive sensors.
Słowa kluczowe: badania nieniszczące , prądy wirowe.

Introduction

The non-destructive techniques (NDT) for the quality control of products are under intensive development since many years and continue to focus much attention in recent times [1]. Eddy Currents Testing (ECT) is one of several methods like, remote field testing (RFT), flux leakage and Barkhausen noise that uses electromagnetic theory to examine conducting materials [2]. Nowadays, with the use of microprocessor based measuring instruments, the potential and user-friendliness of eddy currents testing has been greatly enhanced [3, 4]. The role of the computer has two different components: one related with the possibility to automate the measuring system (control the data acquisition process, process data, signal classification and displaying) and other with numerical modeling of the testing process. In this case the computing capabilities are used to quantitatively predict eddy current signals for realistic situations and to evaluate crack profiles from testing signals by solving the inverse problem of the physical phenomenon under test.

The point is that experimental data cannot be easily interpreted and related to the defects that may be present in the specimen under test. The solution of the inverse problem is an ill-posed problem, thus to obtain a unique solution, patterns must be classified and bi-univocally correlated with the different types of material defects. The idea is to exploit the a priori knowledge of the problem and thus select the proper defect model. In order to investigate the assumptions of the technique, particularly, patterns identification, a huge amount of data is essential and experimentation is necessary.

This paper deals with the measuring interface to be included in an automated microcomputer based ECT system developed to inspect aluminum plates [5, 6]. The probes that impose different distributions of alternating currents flowing in the specimen under test are described and the experimental results obtained with them compared. By inspecting the results, different types of probes allow to recover different types of information necessary to the geometrical characterization of structural defects.

Experimental setup

Figure 1 shows the experimental setup of the measuring system implemented to detect defects in a plate using eddy current testing.

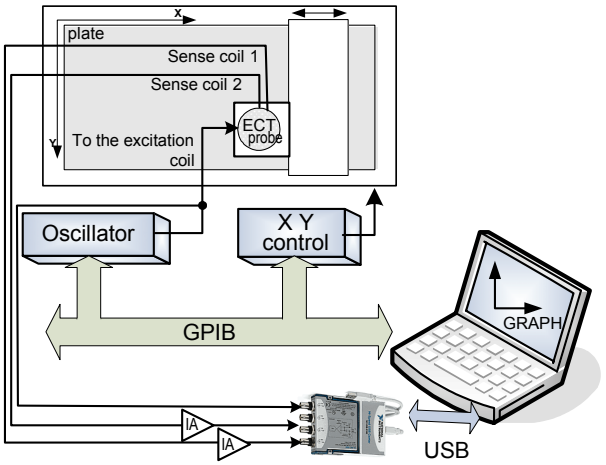

Fig.1. Diagram block of the data acquisition system.

The Eddy Current Testing (ECT) probe scans a conductive aluminium aircraft plate and the e.m.f. due to the magnetic field generated by the currents into the plate are measured using a multifunction data acquisition board (NI cRIO-9215) controlled by the USB port of a PC. This board has four 16 bit resolution simultaneously sampled analog input channels and an input range of 10V. Maximum sampling rate is 100 kHz per channel. In order to obtain higher resolution two high precision instrumentation amplifiers with x100 gain are placed before the A/D converter.

A 5 V RMS, 0-20 kHz oscillator with a power amplifier excites the probe. The excitation current is sampled by the data acquisition board using a 220Ω sensing resistor.

A dual voltage source with a GPIB interface is used to control the automated positioning system implemented using the XY plotter with the probe attached.

ECT Probes

The geometric shape of the sensors is represented in Fig.2. In both probes the excitation coil is driven by a low frequency sinusoidal current and induces electromotive forces in the plate beneath. The detection coils are positioned for both probes also in a symmetric way in order to eliminate the excitation field from the detected signals. However in the presence of a perfect (without flaws) metallic plate, the probe (a) hereafter named tall probe, will sense different voltages in the two detection coils, while the

probe (b) hereafter named flat probe [7], will sense the same voltage in both detection coils.

In the tall probe the two sensing coils are one above the other and coaxial with the excitation. The inner sensing coils diameter is 2 mm and their height is 5.5 mm with a 1 mm gap. The sensing coils have 400 turns using a 0.05 mm diameter copper wire. The excitation coil has 240 turns and uses a 0.18 mm diameter copper wire.

In the flat probe the inner sensing coils diameter is 2.4 mm and their height 9 mm. They are equidistant of the excitation coil axis and separated apart 5 mm. The sensing coils have 500 turns using a 0.05 mm diameter copper wire. The excitation coil has 400 turns and uses a 0.5 mm copper wire.

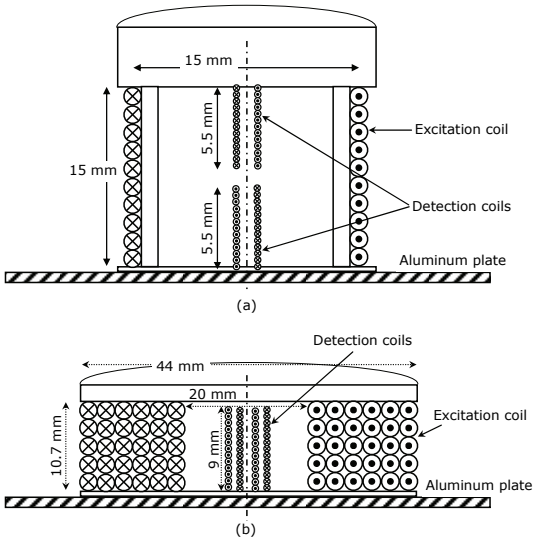

Fig.2. Geometric shape of the inductive sensors. (a) With the detection coils along the axis. (b) With the detection coils parallel to the axis.

Signal processing

Degradation of the measured signals is overcome by digital signal processing.

Some basic digital processing techniques have been used to remove noise and correct the lift-off. Figure 3 shows the flowchart of the actions performed on the raw measured data to obtain the phasors and the contours for the equal level voltage graphs.

Data are acquired during some periods of the excitation current at the maximum sampling frequency of the board. The input signals are the excitation current and the output voltages of the two sensing coils. In order to keep more information on the signals involved, it was decided to acquire the voltages in the two detecting coils separately, subtracting them only after processing. After being filtered, data acquired from the sensing coils are adjusted using a seven-parameter sine fitting algorithm [8]. This method uses the data from both channels to estimate the sine amplitudes, phases, DC components and common frequency, reducing the uncertainty of the estimated parameters. The 7-parameter sine-fit is used instead of the traditional sine-fitting algorithms because it can estimate the parameters of two common frequency acquired signals with lower uncertainties by using the acquired samples of both channels to estimate the common frequency.

With the sine wave amplitudes and the phases of both channels the difference between the output voltages of the sensing coils is computed. The output value corresponds to the data containing the information about the conductivity of the plate. This value is correlated with the voltages that control positioning system and are collected in a matrix indexed to the XY position.

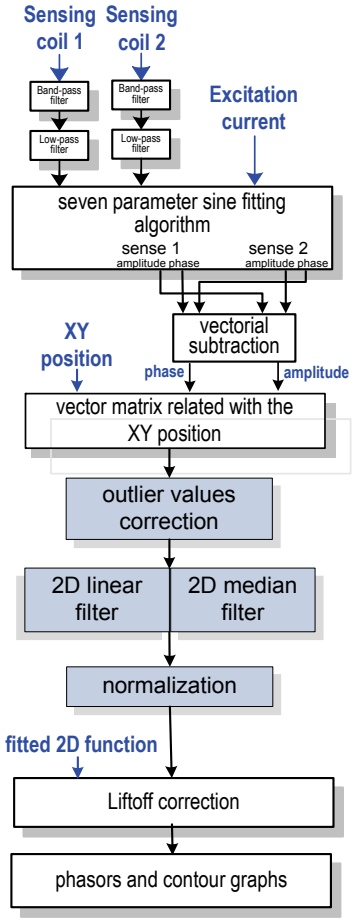

Fig.3. Pre-processing algorithm.

To represent results some more data processing is useful. Filters may be included to remove individual data points (outlier values correction) or all data points that do not fulfil a certain criterion. These processing algorithms were implemented using the MATLAB toolboxes. After performing these actions to the measured data and lift-off correction [6,9] an application to visualize data can be run.

Sensor modelling

To design the sensor, preliminary modelling work must be done in order to preview the field magnitudes and the resulting output voltages in the detection coils [9]. These output voltages are determined with the probes isolated, when there are no conductors in the close vicinity, or in the presence of the metallic plate under inspection without defects. This simulation also allows determining the excitation current amplitude necessary to obtain a given signal to noise ratio as the determined voltages are proportional to the excitation current and the noise is independent of it.

Field equation

The basic equations to be solved are the Maxwell's equations together with the constitutive relationships. To solve these equations the fields are usually represented in terms of different potentials. In eddy-current modelling the magnetic vector potential *A*, and the scalar electric potential *V* are often chosen to solve this kind of problems [10]. However, due to the axisymmetric geometry of the sensor there is no need to include the electric scalar potential V,

because the total electric field will be purely solenoidal as the current density on the interface plate-air is purely tangential, and the conducting material is assumed homogeneous. It is important to remind that this situation is broken when the plate is inhomogeneous, due to the presence of flaws. Maxwell equations are solved taking into account the adequate boundary conditions.

Finite Element Modelling

The finite element model was applied to the geometry represented in Fig. 4 which represents a cross-section of the tall probe.

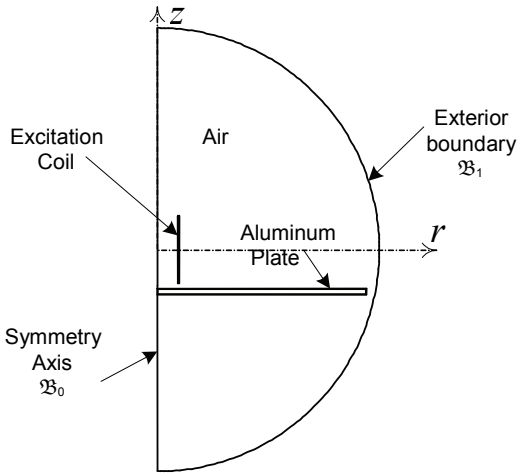

Fig.4. Geometry for FEM application.

Due to the axisymmetric nature of this problem, the cylindrical coordinate system is the most adequate. The magnetic vector potential A_ϕ has a single azimuthal component , and the electric field or the current density have one only component as well.

(1) $$\mathbf{A} = A_\phi \mathbf{u}_\phi \;;\; \mathbf{E} = E_\phi \mathbf{u}_\phi \;;\; \mathbf{J} = J_\phi \mathbf{u}_\phi$$

Maxwell equations written for the case of harmonic fields in terms of the potential **A** assume the form,

(2) $$\nabla \times \nu \nabla \times \mathbf{A} + j\omega\sigma\mathbf{A} = \mathbf{0}$$

(3) $$\nabla \times \nu \nabla \times \mathbf{A} = \mathbf{J}_s$$

being (2) valid inside the aluminium plate and (3) in the region where the source currents are imposed, i.e. the cross section of the excitation coil.

The boundary condition imposed along the symmetry axis B_0 is a Dirichlet homogeneous condition. On the contrary, on the exterior boundary B_1 a mixed condition was used to overcome the open boundary situation. This condition states a linear combination between A_ϕ and its normal derivative along the boundary:

(4) $$\frac{1}{\mu_0}\frac{\partial A_\phi}{\partial n} + C\,A_\phi = 0$$

If A_ϕ is represented in spherical coordinates (r, θ) as

(5) $$A_\phi(r,\theta) = \sum_{k=1}^{\infty} \frac{a_k}{r^k}\cos(k\theta + \alpha_k)$$

an asymptotic approximation can be used, considering only the first harmonic in (5):

(6) $$A_\phi(r,\theta) \approx \frac{a_1}{r}\cos(\theta + \alpha_1)$$

Replacing (6) in (4) it is possible to obtain the value of the constant *C* in (4) in terms of the radius r_0 of the exterior boundary B_1:

(7) $$C = \frac{1}{\mu_0 r_0}$$

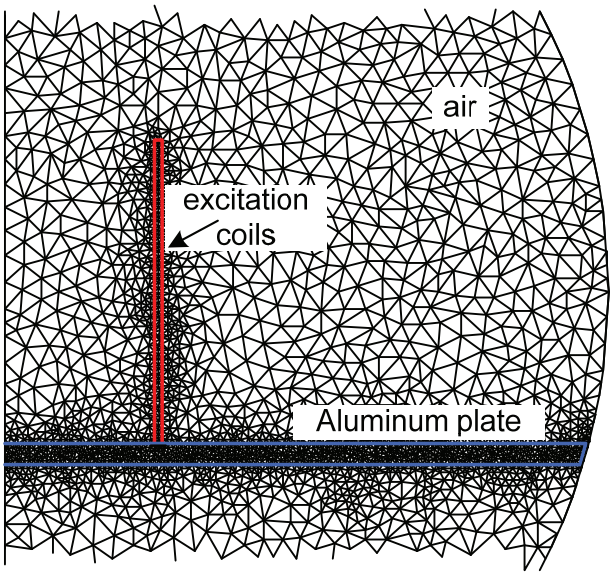

Fig.5. Mesh fragment for FEM application.

The region represented in Fig. 4 was meshed as represented in Fig. 5 using a Delaunay triangulation. With the plate inserted the mesh has 3482 nodes and 6780 elements. The FEM processor was run after insertion of the adequate parameters for frequency, material properties and boundary conditions. The modelling process was run for the tall probe and for the flat probe geometries.

Operating Frequencies

The standard field penetration depth δ varies with frequency ω, material permeability μ and conductivity σ according to:

(8) $$\delta = \sqrt{\frac{2}{\mu\omega\sigma}}$$

An adequate choice of the operation frequency range allows the determination of the ratio of field amplitudes on the upper and bottom surfaces. Previous tests have shown that a good criterion for choosing the operation frequency is the depth of penetration in comparison with the plate thickness. A depth of penetration approximately equal to the plate thickness δ =1 mm, was chosen which corresponds to an operating frequency f =7 kHz. Lower frequencies imply lower output voltages values and higher frequencies only allow the detection of superficial defects.

Figure 6 show the magnetic flux lines obtained for the tall probe geometry with the plate. It shows that almost the total flux is in the upper side of the plate. By a careful examination of this figure it can be seen that the line of the magnetic flux density under the plate corresponds to a reversed sense. This means that inside the plate, the eddy

currents are reversed in relation to the current in the exciting coil.

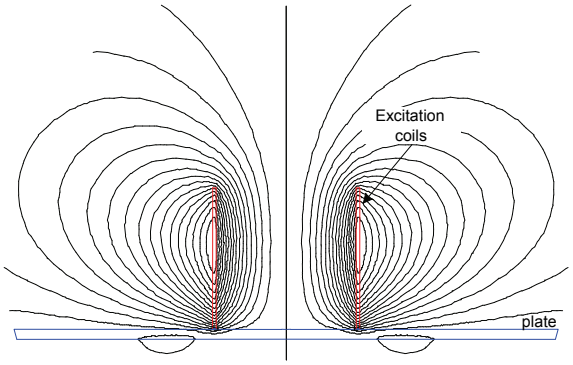

Fig.6. Magnetic flux lines with aluminium plate at f=7 kHz.

Finite Element Modelling

The detection of flaws inside the plates is accomplished by the analysis of the voltages at the terminals of the two detection coils. In Fig.7 two magnetic flux density profiles taken at f = 7 kHz are represented for each probe, one obtained without the plate inserted and another with the plate inserted. The z-axis origin is the plate position. For the tall probe the profiles are calculated along the symmetry z-axis and, for the flat probe the profiles are taken along an axis at a distance d = 3 mm from the probe central axis. The voltages on the detection coils are determined from these profiles via the Maxwell induction law.

For the tall probe when the plate is not present the magnetic flux density is symmetric around z = 6 mm, and the voltages in the two coils are equal. When the aluminium plate is present the magnetic flux density becomes asymmetrical as depicted and the two voltages will be different as well. Data represented was obtained considering that in the 240 turns of the excitation coil, a current with intensity I_{ex}= 8 mA is imposed. From the finite element processor we obtained the average magnetic field inside each one of the detection coils, and the detection coil voltages presented in Table 1. For each one of the sensing coils the magnetic induction flux is approximately. This flux is compatible with a voltage with no plate inserted. When the plate is placed those voltages drop, being the voltage drop in the lower detection coil stronger.

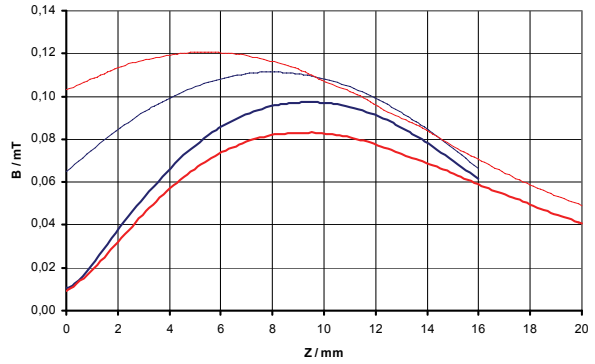

Fig.7. Magnetic flux density profiles along the symmetry axis of the probes for the frequency f =7 kHz. The dashed curves were obtained without the plate and full curve with the plate inserted, being the “upper” curves (1,2) for the tall probe and the “lower” curves for the flat probe.

For the flat probe a symmetry around z = 5.35 mm can be observed when the aluminium plate is not present. When the plate is placed, the lower curve emerges as a consequence of a very low field near the plate. The output voltages were computed considering that in the 400 turns of the excitation coil the same current is imposed and results are presented in Table 1.

Table 1. Output Voltages for Probes with I_{ex}=8 mA@7 kHz

		Detection coil	Experimental Voltage (mV)	Voltage model (mV)	(°)
Tall Probe	No Plate	Upper	7.5	7.6	90
		Lower	7.5	7.6	90
		Difference	--	0	
	With Plate	Upper	6.4	6.9	88.9
		Lower	5.8	5.3	85
		Difference	--	1.65	101.5
Flat Probe	No Plate		10.5	11.5	90
	With Plate		5.0	4.54	12.3

In the flat probe the two voltages in the detection coils are always equal, with or without plate, if the symmetries are maintained and if the plate is homogeneous.

Experimental results

The specimen under test is an aluminium aircraft plate with the length of 29 cm, 14.5 cm width and a thickness of 1 mm. On this plate there are artificial defects with different depths and widths as depicted in Fig. 8. All of them have 23mm length; 2nd, 4th and 6th defects have 0.5 mm width; 1st, 3rd and 5th have 1 mm width; 1st and 2nd perforate the plate and others go half the plate’s thickness.

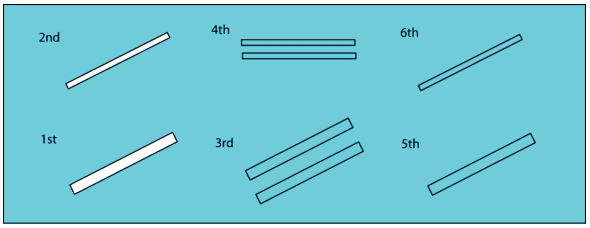

Fig.8. Defects of the aluminium plate under test.

Measurements with the Tall Probe

Figures 9 and 10 represent the contour plots of the normalized voltage amplitudes and an arrow representation of the normalized amplitudes and phases of the output voltages of the two coaxial sensing coils of the tall probe when a scanning of the plate above the 2nd defect is tested.

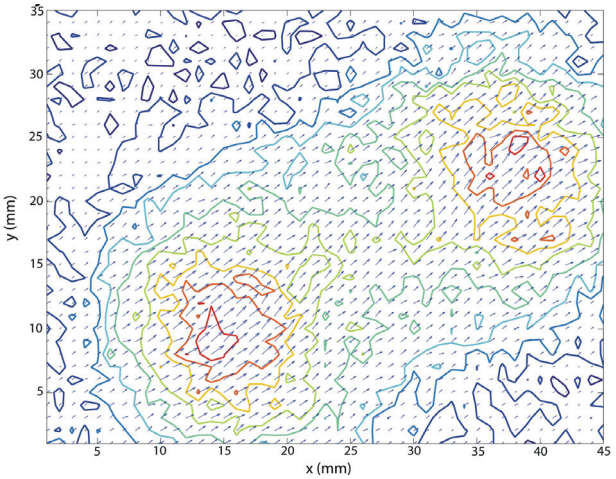

Fig.9. Contour plots of the normalized voltage amplitudes and an arrow representation of the normalized amplitudes and phases of the output voltage of the upper sensing coil.

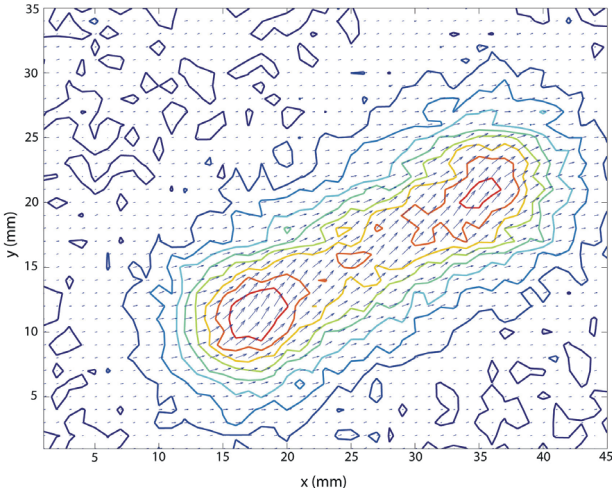

Fig.10. Contour plots of the normalized voltage amplitudes and an arrow representation of the normalized amplitudes and phases of the output voltage of the lower sensing coil.

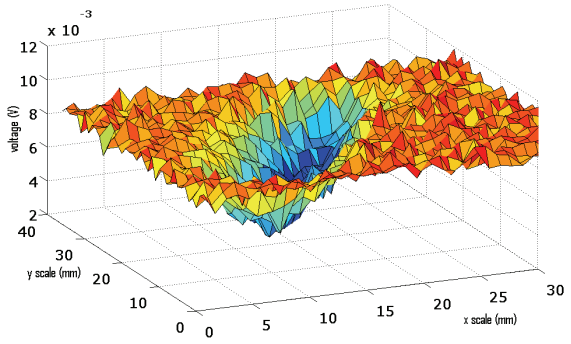

Fig.11. Amplitude of the voltage difference of the output voltages of the sensing coils after sine fitting.

Figures 11 presents the amplitude of the vectorial difference computed from the parameters of the sinus signals determined using the 7-parameter sine fitting algorithm to process the raw data depicted in Figs 9 and 10. No interpolation or filtering was applied. It is clear from this result that the field profile represented can be used separately to localize the wide defects in the plate.

Measurements with the Flat Coil

Figures 12 and 13 represent the contour plots of the normalized voltage amplitudes and an arrow representation of the normalized amplitudes and phases of the output voltages of the flat probe when a scanning of the plate above the same defect is tested.

The scan is executed running parallel lines to the plate edge 1 mm apart. Measurements are taken simultaneously every millimetre over the area of interest when the run from left to right is being executed. As the two sensing coils are put parallel to the edge of the plate, it is always the same coil that meets the defect first, and it is always the other coil that last leaves the defect.

Although improvements in the interpretation of the data taken with the probe with the two sensing coils put side to side are still necessary, some conclusions can be taken from the results depicted. Figure 14 presents the amplitude of the phasors difference presented in Figures 12 and 13. In this probe the sensing coils experience the same total magnetic field when the plate is homogeneous. The output voltages for each coil are the same and the difference is null.

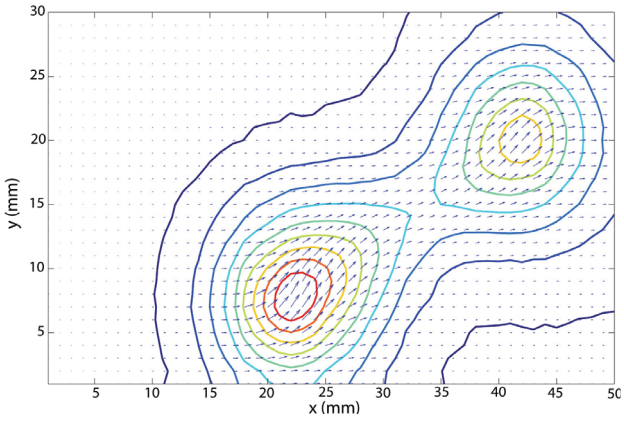

Fig.12. Contour plots of the normalized voltage amplitudes and an arrow representation of the normalized amplitudes and phases of the output voltage of the right sensing coil.

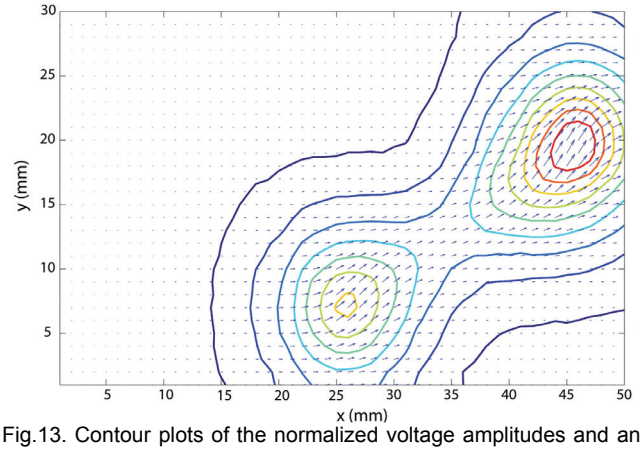

Fig.13. Contour plots of the normalized voltage amplitudes and an arrow representation of the normalized amplitudes and phases of the output voltage of the left sensing coil.

When the probe stands above a defect the output voltages due to the primary (excitation) magnetic field are still equal. However, due to the eddy currents, the secondary magnetic field is distorted and affects differently each coil. If the defects are symmetrical to the two sensing coils no difference voltage is produced. This phenomena justifies the image symmetry depicted in Fig. 14 and may be explored to determine the lengths of cracks.

The higher intensity near the defect edges is due to the enhanced strength of the eddy currents in these regions and is observed on both probes (tall and flat)

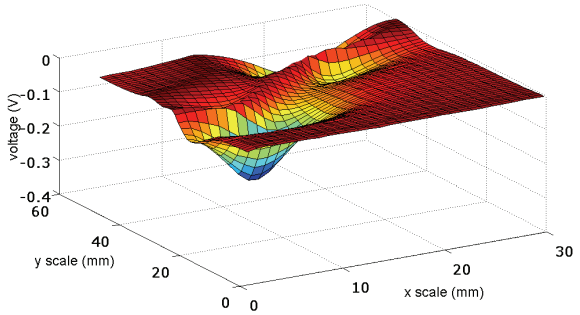

Fig.14. Amplitude of the voltage difference of the output voltages of the sensing coils after sine fitting.

Conclusion

In the paper a data acquisition system to search for defects in metallic nonmagnetic plates was presented. Two types of inductive probes were used. The experimental

setup and the measurement procedures carried out to test the probes are also presented. After some basic signal processing the data profiles obtained are related to the conductivity distribution in the plates. The data obtained allow us to compare the performance of the two types of probes.

The first conclusion is that the flat probe is much more sensitive that the tall probe, indicating that any new probes to be constructed will be as flat as technically possible. In fact being the excitation current in the close proximity of the conductive plate the primary field will be stronger and the induced currents will be stronger as well.

The second conclusion concerns the relative position of the sensing coils. By acquiring the voltages at these two coils separately it is possible to compare them. Thus we conclude that the mean value of the two voltages is related to the normal component of the current density rotational (currents curling in the horizontal plane). The difference of the two voltages is related to one horizontal component of the current density rotational (currents curling in a vertical plane perpendicular to the metallic surface). These last conclusions indicate that in any flat probes to be constructed two pairs of sensing coils may be included to discriminate between these horizontal components.

The obtained results encourage the development of this work. In the next future we intend to proceed with a 3D finite element analysis in order to preview a more accurate shape of the fields and the corresponding induced voltages. This future work will help to invert the problem: to characterize the material defects starting from the measured patterns.

Acknowledgement

This work was supported in part by Portuguese Science and Technology Foundation Project PTDC/EEA-ELC/67719/2006 and in part by the Instituto de Telecomunicações – project CLASSE. This support is gratefully acknowledged.

The authors thank Mr P. Ježdík and Mr J. Neškudla for their preliminary work within the area supported by research program No. MSM6840770015.

REFERENCES

[1] T. Sollier, D. Prémel, D. Lesselier, editors, *Electromagnetic Nondestructive Evaluation* (VIII), Studies in Applied Electromagnetics and Mechanics 24, IOS Press, 2004.

[2] Paul McIntire, *Electromagnetic Testing: Eddy Current, Flux Leakage and Microwave Nondestructive Testing (Nondestructtive Testing Handbook, Vol.4)*, American Society for Nondestructive Testing, 1986.

[3] P. Gaydecki, I. Silva, B. T. Fernandes, Z. Z. Yu, A portable inductive scanning system for image steel-reinforcing bars embedded within concrete, *Sensors and Actuators*, vol. 84, pp. 25-32, 2000.

[4] G. Miller et al., A combined Q and heterodyne sensor incorporating real-time DSP for reinforcement imaging, corrosion detection and material characterization, *Sensors and Actuators* A, vol. 121, pp. 339-346, 2005.

[5] A. Lopes Ribeiro, H. Geirinhas Ramos, Inductive Probe for Flaw Detection in non-Magnetic Metallic Plates Using Eddy Currents, *Proc. I2MTC-IEEE International Instrumentation and Measurement Technology Conference*, Victoria, Canada, pp.1447-1453, 12-15 May, 2008.

[6] H. M. Geirinhas Ramos, A. Lopes Ribeiro, P. Ježdík and J. Neškudla, Eddy Current Testing of Conductive Materials, Proc. *I2MTC-IEEE International Instrumentation and Measurement Technology Conference*, Victoria, Canada, pp.964-970, 12-15 May, 2008.

[7] S. Sharma, L. Udpa, Y. Sun, S. Upda, A modified differential pickup reflection probe, *Review of Progress in Non Destructive Evaluation*, Vol. 17, 1998.

[8] Pedro M. Ramos, Fonseca da Silva and A. Cruz Serra, Improving sine-fitting algorithms for amplitude and phase measurements, *XVII IMEKO World Congress*, Dubrovnik, Croatia, pp. 614-619, June 2003.

[9] P. Jezdik, J. Neskudla, H. M. Geirinhas Ramos, A. Lopes Ribeiro, Classification of Typical Mechanical Cracks in Aircraft Materials Using ECT, *ISEF 2007*, Prague, Czeck Republic, 2007.

[10] O. Bíró, K. Preis, On the Use of the Magnetic Vector Potential in the Finite Element Analysis of Three-Dimensional Eddy Currents, *IEEE Transactions on Magnetics*, Vol.25, N.4, pp.3145-3159.

***Authors**: prof. Helena G. Ramos, prof. Artur L. Ribeiro, Instituto de Telecomunicaçoes, Instituto Superior Tecnico, Av. Rovisco Pais 1049-001, Lisboa, email: hgramos@ist.utl.pt; Ing. Michal Kubinyi, Diagnostics, Nondestructive Testing and Signal Processing laboratory, Department of Measurement, Czech Technical University, Faculty of Electrical Engineering, Technicka 2, 166 27 Prague email: michal.kubinyi@fel.cvut.cz.*